

Engineering Critical Assessment for a Sandwich Pipe Field Joint

Ikechukwu Onyegiri, Maria Kashtalyan*

Centre for Micro- and Nanomechanics (CEMINACS), School of Engineering, University of Aberdeen,
Fraser Noble Building, Aberdeen AB24 3UE

*Corresponding author: m.kashtalyan@abdn.ac.uk

Abstract

This paper seeks to apply a combination of techniques with the aim of outlining a finite element (FE) based methodology for carrying out Engineering Critical Assessment on the swage weld for J-lay installation. The critical potential defect position during installation is identified and its severity is evaluated using the Stress Concentration Factor (SCF). Closed-form parametric equations for quantifying the geometric SCF as a function of the swage weld dimensions are derived using large-scale parametric studies and statistical analysis for the joint under tension. The maximum allowable defect size for a swaged weld under potential installation loadings is evaluated by two proposed FE-based fracture mechanics methodologies. In the absence of tearing resistance data, the influence of the filler resin stiffness, loading type and material response on the acceptability of a defect size is studied and the conservative nature of brittle fracture design for the fracture assessment of carbon steel pipelines with significant ductility is illustrated.

Keywords

Swage weld; J-lay installation; finite element modelling; stress concentration; closed-form equation

1. Introduction

The qualification of field joints and end fittings for any offshore pipeline project involves the determination of limit states for the joint assembly prior to its installation. Experimental and numerical setups are used to conduct full-scale tests to this effect. Typical tests include the limit state testing for joint bending, hydrostatic pressure, internal pressure, thermal expansion and fatigue loads. Most setups accommodate the combination of loadings to simulate live operation scenarios. Experimental procedures are usually developed and standardized after design optimisation has been carried out by the means of Finite Element Analysis (FEA). Experimental procedures are cost intensive and represent a leap to full practicability of the modelled joint whilst being a tool of comparison for numerical models. This comparison helps in refining numerical methods to be more reliable in view of setting up a “virtual testing laboratory” for the analysis of pipe joints (Vitali et al., 1999). This ensures that the operator is fully aware of the critical loading regimes that can affect the integrity of the pipeline system.

Some forms of analytical solutions exist for predicting pipeline joint limit states for use in fracture assessments. These closed form analytical solutions tend to be very conservative and most likely not represent the true nature of the limit states for a pipeline joint, with the margin of error increasing with the complexity in joint geometry and number of components (Bai et al., 2005). To account for the limit states of a sandwich pipe joint, one would need to apply more advance modelling techniques, which will provide flexibility to predicting the effects of a small change to joint profile on the mechanical response, and as such derive limit states from such models. Industry wide, FEA has been utilised to meet this challenge, having a good track record (DNVGL-RP-F108, 2017) (Mallik et al., 2013).

For swaged joints, a qualification plan for testing any design must be developed and qualified in compliance with (DNV-RP-A203, 2011). Research into the mechanics of this joint type proves that the integrity of the swaged weld ensures the structure integrity of the whole pipe-in-pipe as well as its thermal properties (Mallik et al., 2013). Non-destructive examination of all welds used to make-up the

joint assembly could include procedures such as sizing accuracy and point of detection that forms the criterion by which the fitness for purpose criteria is determined (BS 7910, 2013). Due to the swage weld geometry, FEA-based Engineering Critical Assessment (ECA) approach is considered more appropriate; analytical approach conventionally employed for girth and fillet welds is not applicable (Jones et al., 2013). The outline of FEA-based ECA is shown in Figure 1.

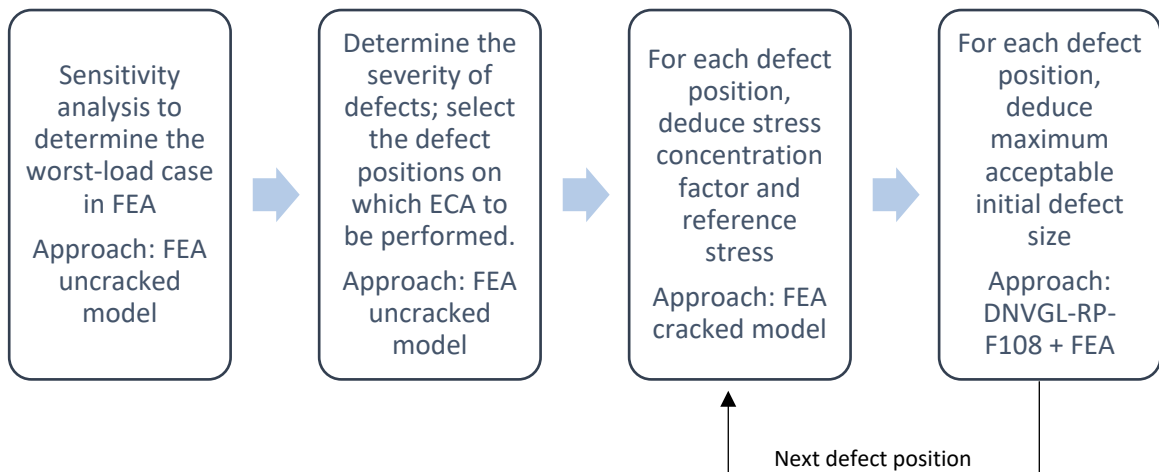
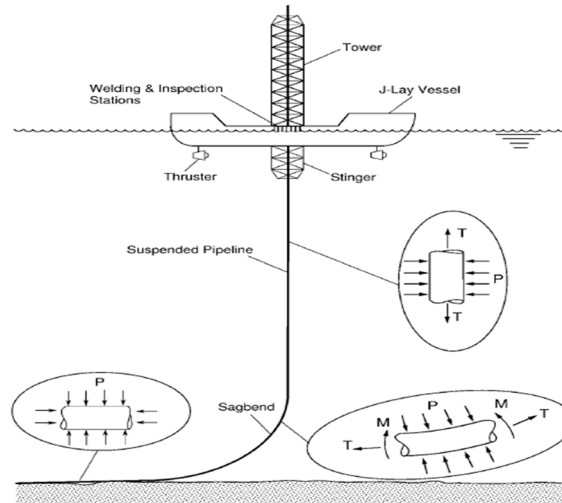


Figure 1 FEA-based ECA

Fracture assessment is the primary tool used to establish weld repair criteria based on static and dynamic loads that may contribute to crack growth whilst ensuring that the crack dimensions do not exceed set critical points that translate to a fracture toughness requirement above that which the material possesses. In other words, fracture assessment seeks to define the fracture limit state based on the stresses applied to a structure and the crack (defect) dimensions. Pipeline girth welds are usually a preferred site for fracture due to stress concentration caused by misalignment, material mismatch, residual stresses as well as and weld flaws (Pisarski, 2011); with focus on circumferentially aligned defects in girth welds, as the loading direction during installation creates stresses normal to the crack face. Figure 2 outlines some of the typical installation loads.



P: Hydrostatic pressure. T: Tension due to pipe weight. M: Moment due to the sagbend curvature

Figure 2 Typical loads on the pipeline during J-lay installation (Kyriakides and Corona, 2007)

2. Theory and Motivation

The fracture mechanics approach is widely used to ascertain the fracture limit state for cracks in pipelines and pipeline girth welds. The applicability of fracture mechanics assessments can be summarised as, firstly, deriving weld defect acceptance criteria and, secondly, evaluating fitness-for-purpose based on the fracture limit state for both installation and operational scenarios. For pipeline girth welds with circumferential defect, the local stress/strain state at the joint should be determined especially in the longitudinal direction as the crack opening is primarily driven in mode I (DNVGL-RP-F108, 2017). This means that a suitable approach must be able to account for the effect of mechanical and geometric factors that affect the stress/strain state at the field joint. This effect can be determined using stress/strain concentration factor solutions as stipulated in (BS 7910, 2013) or by using FEA (Bjerke et al., 2011).

To carry out a generic fracture assessment for monotonic loading using the fracture mechanics approach, as a basic requirement, we need to know some inputs such as: primary membrane and bending stress, pipe/weld dimensions and tolerances, tensile properties (engineering stress-strain curve) of pipe and weld material, critical fracture toughness, stress/strain concentration factor,

maximum acceptable stable crack extension and residual stresses. The required inputs vary depending on the pipeline geometry, loading scenario, environmental conditions and proposed lifetime of the pipeline. Another important consideration is as to whether the approach is defined for load-based or displacement-based installation conditions. Generally, scenarios where the maximum longitudinal stress in the pipe exceeds 90% of the yield stress ($0.9\sigma_y$) are classified as strain-based and below $0.9\sigma_y$, are classified as stress-based.

Assessment is generally made by means of a Failure Assessment Diagram (FAD) based on the principles of fracture mechanics. The FAD (Figure 3) assesses a flaw size against a failure assessment curve, signifying if the flaw is acceptable or not for a particular loading case. The assessment points are plotted using the fracture ratio K_r as the abscissa and the load ratio L_r as the ordinate, derived for the particular load case. The fracture ratio compares the applied loading and can be written explicitly as:

$$K_r = \frac{K_{eff}}{K_{mat}} \quad (2.1)$$

where K_{eff} is the effective stress intensity factor and K_{mat} and is the fracture toughness of the material. The effective stress intensity factor is computed from the stress intensity factor solutions derived from FEA as

$$K_{eff} = \sqrt{K_I^2 + K_{II}^2 + \frac{K_{III}^2}{(1 - \nu^2)}} \quad (2.2)$$

where K_I, K_{II} and K_{III} represent the Stress Intensity Factors (SIF) corresponding to mode I, II and III respectively.

The load ratio L_r is computed as:

$$L_r = \frac{\sigma_{ref}}{\sigma_y} \quad (2.3)$$

where σ_{ref} is the reference stress and σ_y is the material yield stress. The reference stress σ_{ref} is an important parameter that allows for the prevention of plastic collapse in a given geometry under certain loading conditions. For static loading, the reference stress is the representative stress for the

annular region from which the Stress Intensity Factor (SIF) solutions are computed and that can be calculated analytically for a number of geometries (BS 7910, 2013), capturing the influence of the primary membrane and bending stresses, flaw dimensions and structure size. For the swaged weld, the reference stress is the equivalent longitudinal stress due to maximum potential loading during installation and can only be computed using FEA.

In order to derive the failure assessment curve, detailed stress-strain data is required especially for strains below 1%. The ordinate of the failure assessment curve points is the load ratio that is computed as the ratio of the engineering stress to the yield stress. The required engineering stress is equivalent to the reference stress in Eqn. (2.3) and is derived from the stress-strain data as a function of the selected load ratio. As a minimum, L_r values should be selected at 0.7, 0.9, 0.98, 1.0 and 1.02. The abscissa of the failure assessment curve points can be derived using the expression for the “Option 2” curve (BS 7910, 2013):

$$f(L_r) = \left(\frac{E \varepsilon_{ref}}{L_r \sigma_y} + \frac{L_r^3 \sigma_y}{2E \varepsilon_{ref}} \right)^{-0.5} \quad \text{for } L_r < L_{r,max} \quad (2.4)$$

$$f(L_r) = 0 \quad \text{for } L_r \geq L_{r,max} \quad (2.5)$$

where ε_{ref} is the true strain at the true stress computed from $L_r \sigma_y$ for the load ratios considered and

$$L_{r,max} = \frac{\sigma_u + \sigma_y}{2\sigma_y} \quad (2.6)$$

where σ_u is the ultimate tensile strength. The “Option 2” curve is suitable for all metals regardless of the stress-strain behaviour as it captures the non-linearity in the stress-strain curve.

In the absence of tearing resistance data for the swage weld geometry, the methodology described above can only be applied when using the Linear Elastic Fracture Mechanics (LEFM) theory and assumptions (Sun and Jin, 2012). In other words, the small-scale yielding assumption is valid for this approach. Small-scale yielding simply implies that the region of inelastic deformation at the crack tip is well within the zone dominated by the LEFM asymptotic solution. This allows for the characterisation of the local crack-tip stress field using solely the elastic stress intensity factor K , which is a function of the applied stress, the location and size of the crack and the geometry of the pipe joint

(Zehnder, 2012). In other words, K defines a stress profile near the crack tip that upon reaching a critical state signifies a small crack extension and subsequent material failure. This critical state is denoted by a value K_{mat} , also known as the fracture toughness of a material (critical value of K required to initiate crack growth). This theory works well for brittle materials; as for ductile materials, we know that the fracture toughness is a function of the crack extension and we would need a tearing resistance curve, where the crack driving force is a function of the crack extension, to appropriately predict stable tearing (Pisarski et al., 2006).

Determining the material fracture toughness measured by J-methods, J_{mat} of a material (Zhu and Joyce, 2012) allows us to obtain the critical fracture toughness for a linear elastic material under quasi-static conditions and plane strain (gives the practical minimum value):

$$K_{mat} = \sqrt{\frac{J_{mat}E}{1 - \nu^2}} \quad (2.7)$$

where E and ν are the elastic modulus and Poisson's ratio respectively.

Calculations for a flaw provide the co-ordinates either of an assessment point or, in the case of crack growth, a locus of points. These points are then compared with the failure assessment curve to determine the acceptability of the flaw. A simple illustration of this methodology for a circumferential crack (of depth a) in a pipe in tension is shown in Figure 3(a), where defects corresponding to assessment points that lie outside the failure assessment curve are deemed unacceptable. For a surface crack in a plate under axial loading, the elastic SIF solutions from FEA show good agreement with analytical solutions (BS 7910, 2013) as illustrated in Figure 3(b).

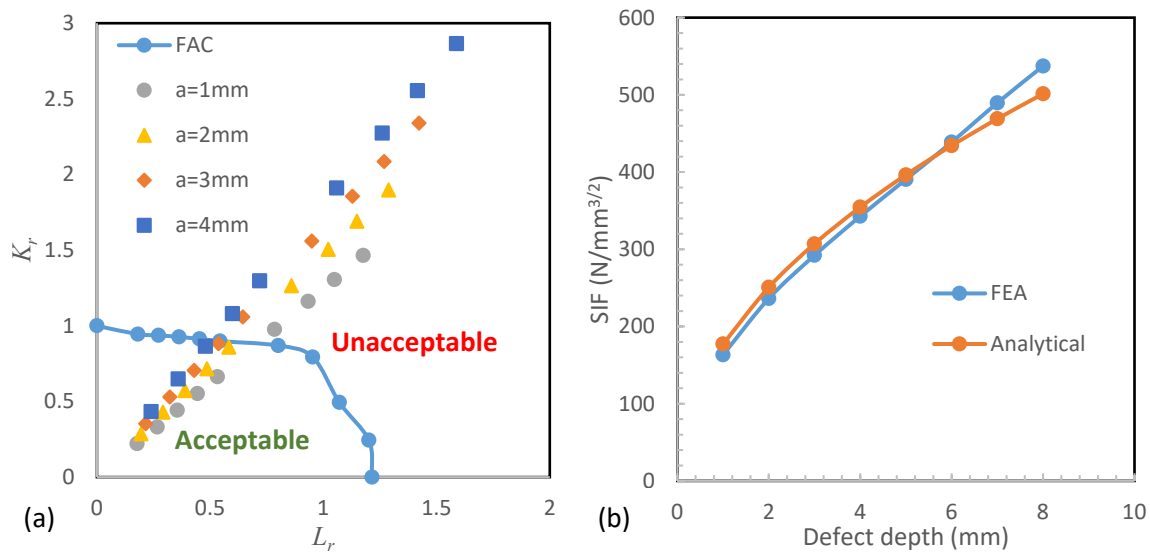


Figure 3 (a) FAD assessment points and a failure assessment curve (FAC) for a pipe with circumferential crack in tension;
(b) Elastic SIF comparison

For pipeline girth welds and tubular fillet welds there exist, in form of codes and standards (BS 7910, 2013, API-579-1/ASME-FFS-1, 2016), a compendium of detailed reference stress and SIF solutions. For the specific geometry of the swage weld, the SIF and reference stress inputs required for the ECA can only be obtained by FEA and as such, the studies carried out in this paper utilise only FEA methodologies. Several studies have applied the FEA approach to arrive at unique solutions to “standard-exempted” problems. In (Bjerke et al., 2011), a simplified procedure was introduced for performing more accurate prediction of the crack driving force based on (DNV-OS-F101, 2007) by using 3D FEA. In (Ostby, 2005), an equation was derived to calculate the applied crack driving force in terms of J-integral or crack tip opening displacement for pipes with surface cracks based on 2D and 3D FEA; taking into account the effect of biaxial loading, yield stress mismatch and misalignment. Using large-scale 3D FEA-based parametric studies, in (Kibey et al., 2010) closed-form strain capacity equations were derived, which were then utilised for strain based design ECA procedures for welded pipelines. In response to the geometric limitations of the stress intensity factor and reference stress solutions as documented for pipe joint types in recommended practice standards, finite element fracture mechanics methods have been long utilised to capture the stress state for different combinations of

defects in unique joint types (Arun et al., 2014, Kibey et al., 2010, Bell et al., 1985). In addition, it is used to confirm the validity and hence conservatism of analytical procedures (Bjerke et al., 2011). No documentation of the utilization of finite element fracture mechanics for the swaged weld has been published and the influence of the core and filler resin load-carrying capacity on the fracture assessment outcomes of the swage weld remains unknown.

This paper seeks to apply a combination of techniques with the aim of outlining a FEA-based methodology for carrying out ECA on the swage weld for J-lay installation. In the first section, in order to avoid carrying out ECA on all potential defect positions, the stress profile at the swaged weld is examined to determine the most severe defect position as a function of the stress concentration. Closed-form parametric equations for quantifying the geometric Stress Concentration Factor (SCF) as a function of the swage weld dimensions are derived using large-scale parametric studies and statistical analysis for the joint under tension. For unique joint types, FEA methodologies can indeed be used to derive such equations (Morgan and Lee, 1998), and such solutions can be considered adequate in the absence of full experimental results. The FEA methodology to determine the crack driving force and the acceptable flaw size for the swage weld in a sandwich pipe joint is outlined based on procedures in (DNVGL-RP-F108, 2017) and (API-579-1/ASME-FFS-1, 2016).

3. Analysis of critical defect position

The distribution of stress about the swage weld toe is known to be a major consideration in both the fracture and fatigue assessment of swaged jointed pipe-in-pipe systems (Mallik et al., 2013). During offshore installation, the sandwich pipe joint would have to withstand the reaction force from the tensioner due to the weight of the submerged part of the pipe assembly and a bending moment at the sagbend just before being laid on the seabed. With respect to these loadings, stress concentration around the swaged weld toe is expected due to the change in geometry and strength mismatch between the weld metal and the pipe metal, all which cause stress discontinuities.

For the sandwich pipe swage joint the geometrically induced stress concentration can be quantified using the so-called Stress Concentration Factor (SCF) defined as:

$$SCF = \frac{\text{maximum stress in region of interest}}{\text{stress in component without stress riser}} \quad (3.1)$$

The geometry of the connection and swaged weld is shown in Figure 4 for a discontinuous annulus joint type (meaning there is no continuous transfer of load between two adjacent outer pipes, only through the swage weld).

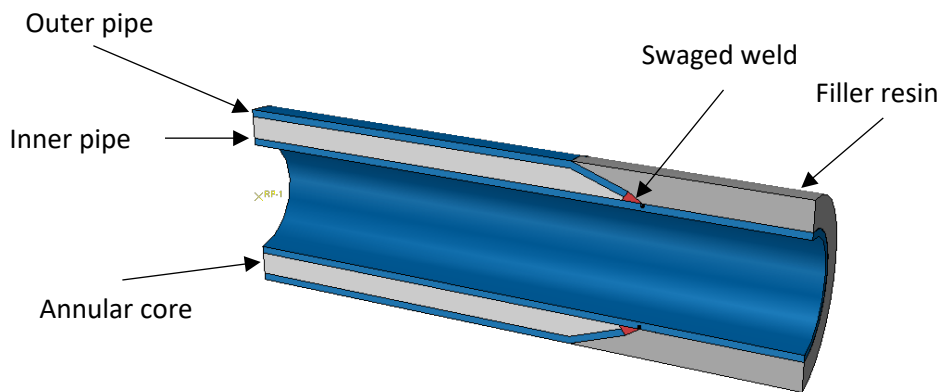


Figure 4 Configuration of a sandwich pipe field joint

The regions must first be classified in order of stress severity under loadings to determine the worst scenario model. For this, a base model is built with properties as stated in Table 1.

Table 1 Properties of base model

	Young's modulus E (GPa)	Poisson's ratio ν	Radius r (mm)	Thickness t (mm)
Inner pipe	205	0.3	109.55	12.7
Outer pipe	205	0.3	161.95	12.7
Swaged weld	207	0.3	n/a	n/a

The entire analysis is based on linear elastic deformation only. Considering a model of the swaged weld joint in tension, we can express a consistent statistical through thickness stress distribution in terms of a membrane component σ_m and a bending component σ_b as seen in Figure 5(a), which add up to give the nominal stress σ_n . The peak stress σ_{peak} can be described as the product of the geometric SCF and σ_n . This represents a local through-thickness normal and shear stress distribution at the swaged weld toe. The potential defect positions as highlighted by (Mallik et al., 2013) are marked in Figure 5(b).

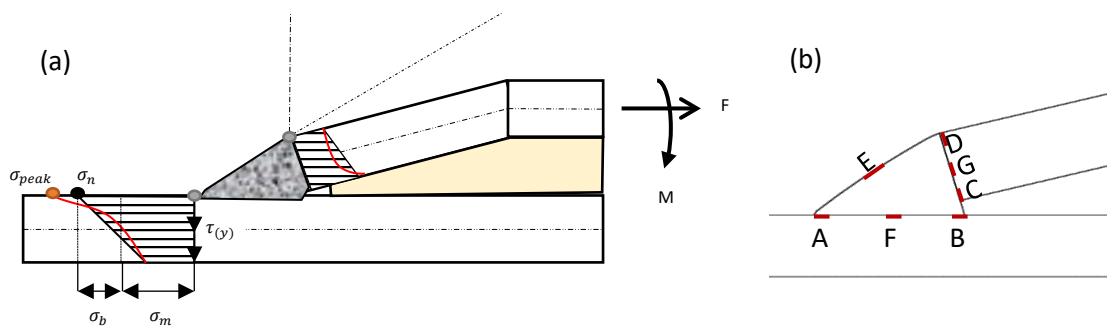


Figure 5 (a) Geometry of the swage weld; (b) Locations for potential defects

Similar studies carried out on a conventional pipe-in-pipe subjected to J-lay installation loads revealed that the weld toe (location A) would experience the highest stress concentration relative to the other locations (Dixon et al., 2003). In preliminary fracture assessment, this location is recognised to be a potential failure location in the presence of fabrication imperfections and is usually taken as the limit region for the joint. This is the first step in the ECA, and for an installation case, the fracture assessment is of more concern to us. Indeed having an idea of the stress distribution and peak stresses that would occur at the swaged weld toe would be a great first step to understanding just how the fracture assessment criteria will be established.

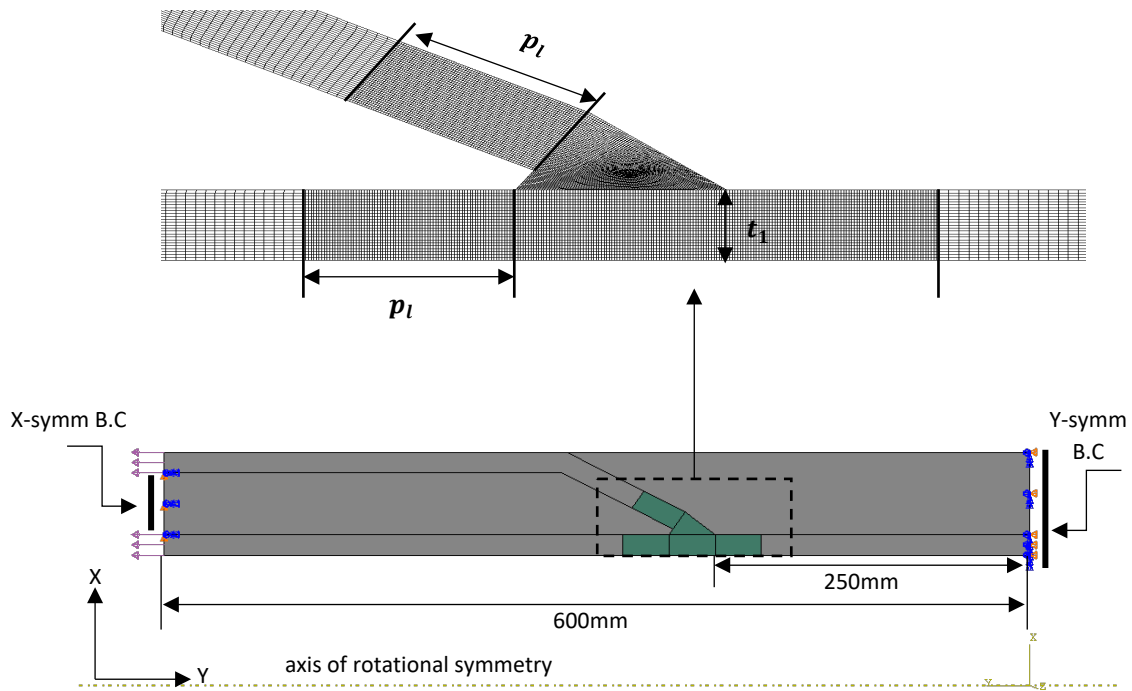


Figure 6 Axisymmetric finite element model

The finite element software ABAQUS (ABAQUS, 2014) was used for all load cases in this study. Under axial loading, the base model was subjected to 60% of its axial capacity as described in (API-RP-1111, 2015), with perfect bonding assumed between the interlayers of the sandwich pipe. Since the geometry and loading of the given case satisfy rotational symmetry, axisymmetric models with CAX4 elements (4-node bilinear axisymmetric quadrilaterals) were used to capture this behaviour. In view of the perfect bonding assumption between the interlayers, one would be able to define the installation tension as an equally distributed force acting at the pipe ends as seen in Figure 6. Geometric partitions were made about the potential defect locations and mesh refinement applied. The partition length $p_l = \sqrt{r_m t_1}$ was chosen as the meridional length for local stress classification as specified in (ASME BPVC-VIII-2, 2015) where r_m and t_1 are the inner pipe mid surface radius and thickness respectively. A generic mesh convergence study was carried out to ascertain the change in the peak stress with mesh density as seen in Figure 7(a). Since the measure of “stress” as we limit the

mesh size to infinitesimal values in elastic analysis will approach infinity and thus unrealistic, an instability criterion was defined in ABAQUS to calculate the Load Proportionality Factor (LPF) at the first instability at the swaged weld region. The mesh density was normalised by its lowest value in the sample set. A typical result can be seen in Figure 7(b), showing the stress distributions around the swaged weld.

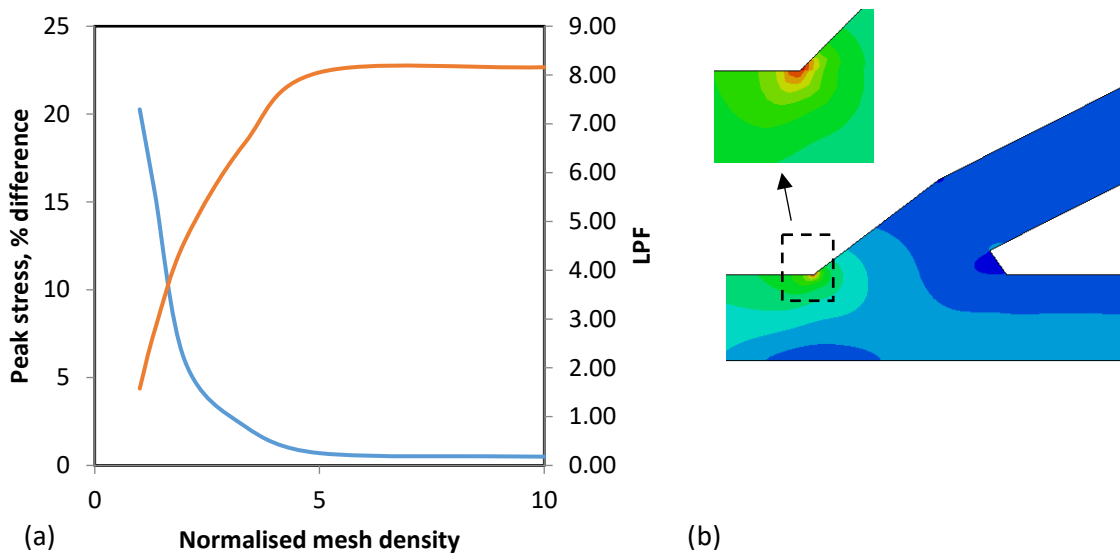


Figure 7 (a) Variation of peak stress with normalised mesh density; (b) Stress contour plot of swage weld (red contour: peak stress)

The stress linearization technique outlined in (ASME BPVC-VIII-2, 2015) was utilised via the stress classification line. The stress classification line for each potential defect position was chosen to be perpendicular to its mode I opening direction. The longitudinal membrane plus bending stress component was computed and compared with results obtained by (Mallik et al., 2013) where the stress severity ranking by location was A, B, C, D. The results obtained in this study can be seen in Table 2.

Table 2 Longitudinal membrane plus bending stress at defect location A, B, C, D

Location	A	B	C	D
Stress (MPa)	398.4	107.9	87.6	62.6

It should be mentioned here that perfect bonding was assumed for all surfaces and as such, interaction effects were not considered. The consistency between the FEA results and the full scale testing (Mallik et al., 2013) verifies the load pathways and localised stress distribution at the swaged weld.

4. Parametric Study

The parametric study is only carried out for the most critical defect position, the swage weld toe (location A). The geometry of the swage weld can be parametrically defined using dimensional constraints as illustrated in Figure 8.

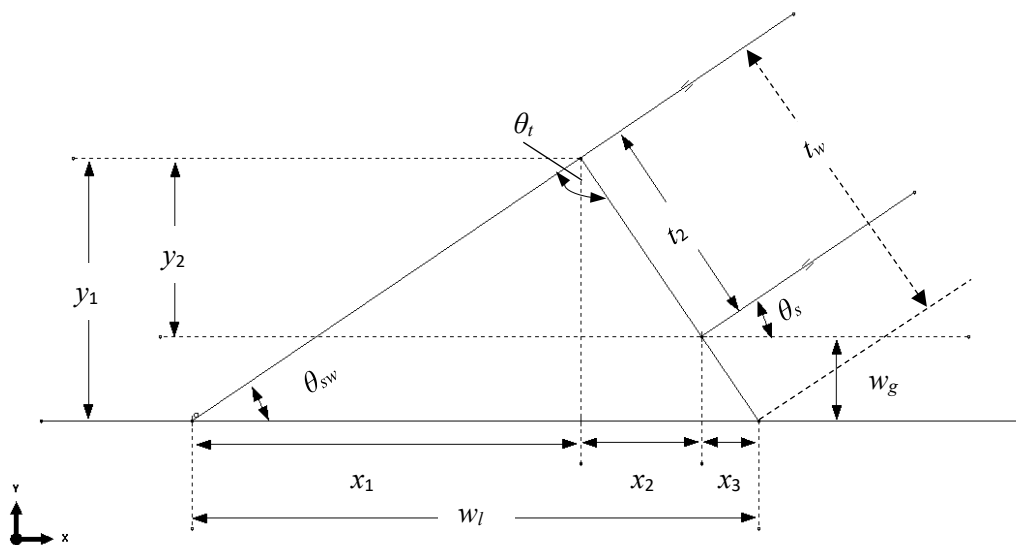


Figure 8 Dimensional profile of swage weld

To ensure that the developed geometry maintained parametric consistency the swage profile was constrained to a dimensional degree of freedom of two:

$$t_w = f(w_l) = f(w_g, \theta_{sw}), \quad \theta_{sw} + \theta_t - \theta_s = \frac{\pi}{2}, \quad w_l = x_1 + x_2 + x_3$$

The resulting geometric equations then become input functions for the parametric scripts

$$y_1 = w_g + \sin\left(\frac{\pi}{2} - \theta_s\right) t_2 \quad (4.1)$$

$$x_1 = \frac{y_1}{\tan \theta_{sw}} \quad (4.2)$$

$$x_2 = t_2 \cos\left(\frac{\pi}{2} - \theta_s\right) \quad (4.3)$$

$$x_3 = \frac{w_g}{\tan\left(\frac{\pi}{2} - \theta_s\right)} \quad (4.4)$$

$$w_l = \frac{w_g + \sin\left(\frac{\pi}{2} - \theta_s\right) t_2}{\tan \theta_{sw}} + t_2 \cos\left(\frac{\pi}{2} - \theta_s\right) + \frac{w_g}{\tan\left(\frac{\pi}{2} - \theta_s\right)} \quad (4.5)$$

$$t_w = t_2 + \frac{w_g}{\sin\left(\frac{\pi}{2} - \theta_s\right)} = w_l \sin(\theta_{sw}) \quad (4.6)$$

The selected range of material and geometric parameters used for parametric study can be found in Table 3. The range of E_{cp} (core-to-pipe elastic modulus ratio), E_{rp} (resin-to-pipe elastic modulus ratio) and E_{wp} (weld-to-pipe elastic modulus ratio) was chosen based on upper and lower bound limits that are practically applicable. The range of w_l (swaged weld length) and w_g (swaged weld gap) was chosen based on reported samples as fabricated by (Mallik et al., 2013).

Table 3 Range of parameters used in the parametric study

E_{cp}	E_{rp}	E_{wp}	w_l (mm)	w_g (mm)	t_1/r_1
0.001	0.001	0.8	25	3	0.12
0.005	0.005	0.9	30	6	0.15
0.01	0.01	1.0	35	9	0.17
0.05	0.05	1.1	40	12	0.20
0.1	0.1	1.2	45	15	

4.1. Influence of swage weld length

The swage weld length w_l is the main design parameter that determines just how much weld metal is deposited to form the connection and is a direct function of the angular difference between the outer pipe swage angle and the swage weld angle. Two different sets of core and resin stiffness are examined with the weld gap fixed in all design models. Figure 9 shows the influence of the swage weld length on the SCF. It can be seen that increasing the weld length reduces the SCF at the swage weld toe. This is directly related to the increased surface area of the weld, meaning it will be able to carry more load. This is obviously a simplistic approach as other fabrication, inspection and geometric tolerances would constrain the actual weld length that can be utilised for a swage connection.

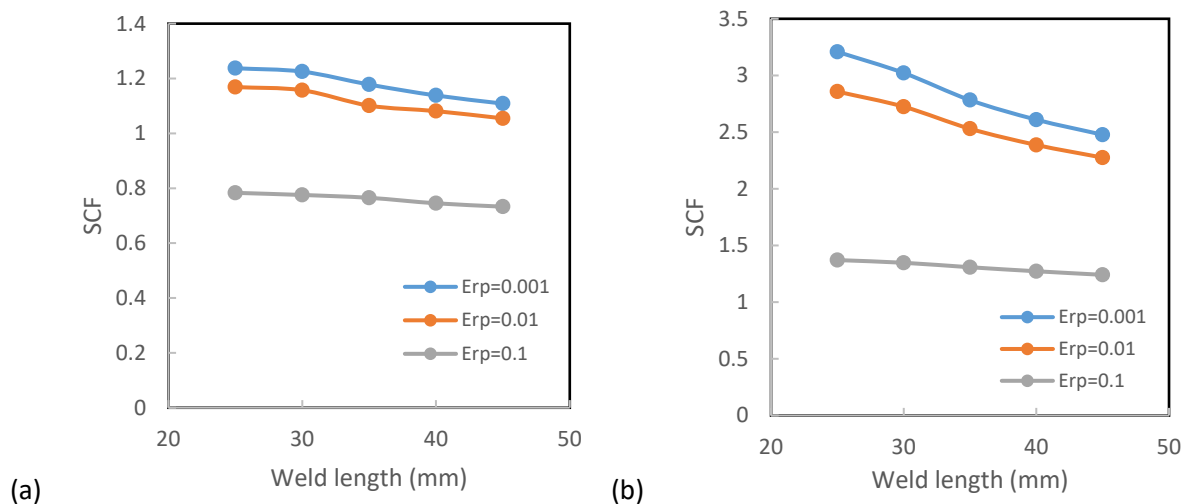


Figure 9 Influence of weld length w_l on SCF for a range of resin-to-pipe elastic modulus ratios E_{rp} :

(a) Continuous annulus; (b) Discontinuous annulus

4.2. Influence of swage weld gap

The weld gap w_g directly influences the evolution of compressive stresses at the throat of the swage weld. These compressive stresses are magnified as the weld gap reduces and have an inverse relationship with the tensile stresses at the swage weld toe. Therefore, as the weld gap increases, the compressive stresses at the throat decreases and this amplifies the tensile stresses around the swage

weld toe (Figure 10). The welding residual stresses would definitely have a significant effect on the stress distribution around the swage weld and should be considered during detailed design of the joint.

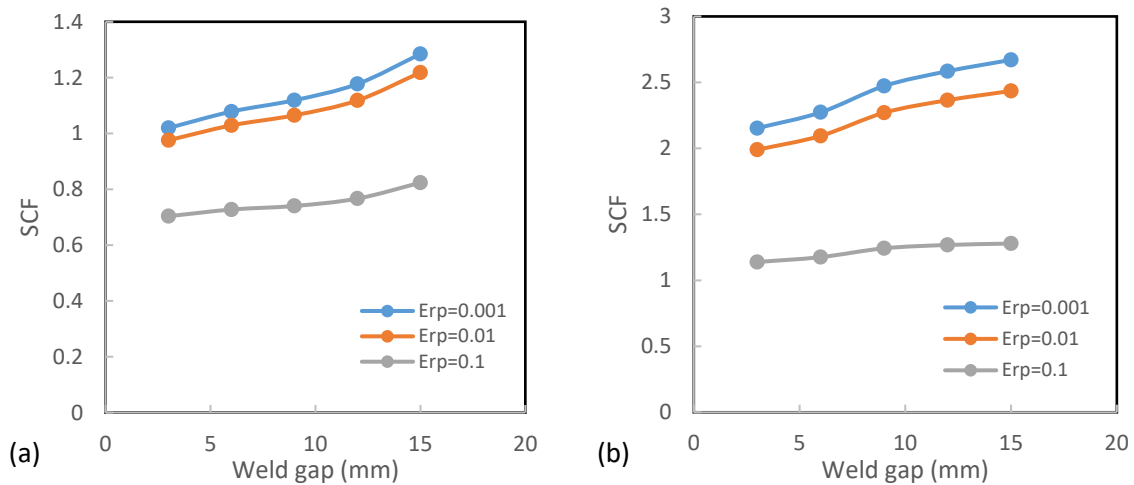


Figure 10 Influence of weld gap w_g on SCF for a range of resin-to-pipe modulus ratios E_{rp} :

(a) Continuous annulus (b) Discontinuous annulus

4.3. Influence of thickness to radius ratio

We can see from Figure 11(a) that the influence of the inner pipe thickness to radius ratio t_1/r_1 on the SCF is as expected. As t_1/r_1 increases, the SCF reduces for all sampled weld lengths, because the pipe's cross sectional area increases also. The stiffer the weld metal, the higher the SCF will be simply due to the preferential deformation of the inner pipe at the interface with the weld (Figure 11(b)). The advantage of having continuous load transfer between adjacent outer pipes can be seen from the results for continuous and discontinuous annulus type joints as the SCF is always lower for continuous annulus joints. Although this requires additional weld connections being made during installation, which subsequently increases the offshore time and the installation cost.

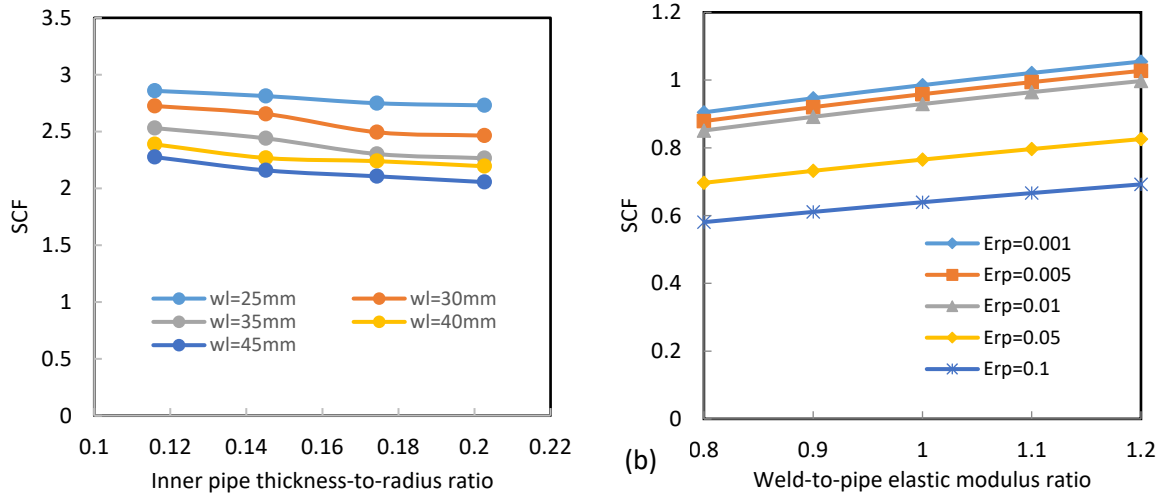


Figure 11 (a) Influence of the inner pipe thickness-to-radius ratio t_1/r_1 on SCF for a range of weld lengths w_l (discontinuous annulus);

(b) Influence of weld-to-pipe elastic modulus ratio E_{wp} on SCF for a range of resin-to-pipe elastic modulus ratios E_{rp} (continuous annulus)

4.4. SCF Correlations

Considering the wide range of geometric parameters involved in the analysis of the stress state at the swage weld, it would be cumbersome to try to develop simple equations that can accurately predict the SCF at the weld toe for all possible configurations. Using the results from 12500 FE models, a set of fitted correlations were derived to predict the SCF at the weld toe and quantify the geometrically induced stress magnification. This approach is only applicable for elastic analysis and axial load cases (e.g. tension due to pipe weight during installation). The below listed correlations exclusively quantify the influence of the geometric and elastic material properties on the SCF and as such the accuracy is not a function of the remote axial loads as long as there is no plastic deformation. In addition, the perfect adhesion assumption holds true for these correlations, hence the transfer of load between pipe-core, pipe-weld and pipe-resin is continuous.

The models were automatically generated using a script file with the geometric parameters shown in Figure 8 and given in Eqns. (4.1) – (4.6) and parameter values listed in Table 3. To arrive at the full model sets, each parameter value in Table 3 is used in combination with other parameters for the

four sampled values of t_1/r_1 yielding $(4 \times 5^5) = 12500$ model sets. A python script file was utilized for the automated model input file generation, creation of an array of input files that varied one parameter against the others and submission of the analysis jobs. A SLURM script (Yoo et al., 2003) was then utilised to run the python script file on a supercomputer cluster. Afterwards, the maximum longitudinal stress values at the swaged weld toe were extracted from the output database file using a predefined node set embedded in a modified python file (compatibility was not a problem as the mesh was the same for all models) run in the python development environment of ABAQUS. The extracted results were then copied to the analysis module of (SigmaPlot, 2014) where the data was fitted to yield correlations to the FE results and generate shared parameters between data sets which are then used to generate scaling factors as a function of the sampled parameter.

Results from the correlations proposed below were compared with results from finite element analysis. To capture the variation of the input parameters extensively, a parameter randomization function was incorporated in the script used to generate the model input files. The variation in both results is seen in Figure 12 for eight random parameter datasets.

The following equations are valid for $1.0 \leq w_L/t_w \leq 2.0$, $0 < w_g/t_w \leq 0.5$:

$$SCF = abce(1 + \frac{w_L}{t_w})^{-d} \quad (4.7)$$

$$a = -3.53 - 2.466 \ln(E_{rp} + 0.01018) \quad (4.8)$$

$$b = \frac{b_{(i)}}{b^*} \quad (4.9)$$

where

$$b^* = 3.7776 \left(\frac{w_L}{t_w}\right)^{-0.631} \quad (4.10)$$

$$b_{(i)} = b' \left(\frac{w_L}{t_w}\right)^{-b''} \quad (4.11)$$

$$b' = 3.097 - 0.1702 \ln(E_{cp} + 0.00831) \quad (4.12)$$

$$b'' = 0.3264 - 0.0777 \ln(E_{cp} + 0.009829) \quad (4.13)$$

$$c = 0.7683(1.941)^{\frac{wg}{t_w}} \quad (4.14)$$

$$d = 1.0233 \exp(-9.526 E_{rp}) \quad (4.15)$$

$$e = 0.2304 \exp\left(11.976 \frac{t_2}{r_2}\right) \left(\frac{t_1}{r_1}\right)^{\left(1.0525 \frac{t_2}{r_2} - 0.2726\right)} \quad (4.16)$$

Through thickness variation

The equation is valid for $1.0 \leq w_l/t_w \leq 2.0$, $r_i \geq r_m$, $\varphi = 1$ for $r_i = r_m$ for all w_l/t_w . Parameter φ defines a stress decay parameter, where the stress at a point r_m is

$$\sigma_{r_m} = \varphi * \text{SCF} * \text{remotely applied stress}$$

$$\varphi = \frac{-1.025 + \left(\frac{r_m}{r_i}\right)}{-f + g \left(\frac{r_m}{r_i}\right)} h \quad (4.17)$$

$$f = 3.8737 \left(\frac{t_1}{r_1}\right)^{0.2124} \quad (4.18)$$

$$g = 3.8513 \left(\frac{t_1}{r_1}\right)^{0.2145} \quad (4.19)$$

$$h = \left(0.2995 \left(\frac{w_l}{t_w}\right) + 0.4765\right) + 0.707 \ln\left(\frac{r_m}{r_i}\right) \quad (4.20)$$

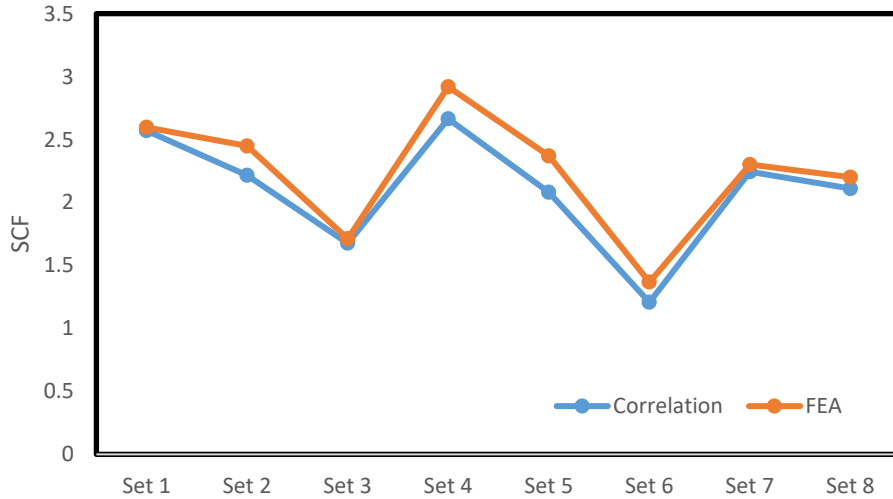


Figure 12 Comparison of correlation and FEA results

5. Fracture Assessment

As was shown in previous sections, for installation-based loadings on the sandwich pipe the critical defect is located at the swage weld toe. Therefore, the results at the swage weld toe are then interpreted as limit indicators for the study of the fracture assessment of the sandwich pipe joint. This study is undertaken for the discontinuous annulus type joint.

5.1. Finite element analysis

As with every finite element approach, the accuracy of the results depend on the model properties. Therefore, it is imperative to ensure that the mesh refinement is satisfactory by means of validation using a mesh convergence study. Mesh refinement should be achieved in such a way that the contour integral is progressive and maps finite regions within acceptable limits in which the LEFM and small scale yielding theories are valid. The choice of elements is equally important, as one should take care to avoid mid-node approximations within the contour integral calculation. A simple formulation to mapping the contour integral regions is shown in Figure 13(a), where r_p is the radius of the plastic process zone (LEFM is not valid in this zone) and r_k is the K-dominance field where LEFM/small scale yielding theories are valid and give a good approximation of the complete stress

field (ABAQUS, 2014). To avoid conservatism, one can define the contour integrals in such a way that it is progressive and bound between these two zones. The FE package ABAQUS was used to undergo all case studies. It offers three different criteria for isotropic linear elastic materials namely: the maximum tangential stress criterion, the maximum energy release rate criterion and the $K_{II} = 0$ criterion. Although these criteria, like most general loading theories, assume that crack extension occurs with $K_{II} = 0$, they do vary slightly with the prediction of crack initiation angle (Dassault Systèmes, 2012). The simplest estimation of the plastic zone size can be obtained from the elastic solution of the sharp crack problem. For characteristic crack length a , the definition of a finite zone r_k in which K-field dominates needs to satisfy the criterion (Dassault Systèmes, 2012):

$$\frac{a}{5} > r_k > 3r_p \approx \frac{1}{2} \left(\frac{K_{IC}}{\sigma_y} \right)^2 \quad (5.1)$$

where K_{IC} is the critical stress intensity factor for mode I fracture and σ_y is the material yield stress.

The computed plastic zone size is based on Irwin's suggestion for mode I fracture (Irwin, 1961).

The J-integral method is also achievable using FE analysis, where for linear elastic materials; the J-value can be used to represent the energy release rate G , associated with crack growth. Applying small scale yielding assumptions, the contour for the J-integral (λ) will fall within the region in which LEFM is valid as shown in Figure 13(a). Thus, for a linear elastic material the following is valid (plane strain):

$$J = G = \frac{1 - \nu^2}{E} K_I^2 \quad (5.2)$$

The theory behind the FE computation of the SIF and J-integral is detailed in (ABAQUS, 2014).

Modelling of the crack within the pipe can be done using a defined seam for sharp cracks with infinitesimal length in the axial direction or a blunt semi-elliptical crack with open geometry as shown in Figure 13(b) for a pipeline girth weld with misalignment. Sharp cracks are best suited for small-strain analysis and care should be taken in interpreting the singularity behaviour at the crack

tip. On the other hand, blunted cracks are best suited for finite-strain analysis, and depending on the defined crack tip profile, non-singular behaviour is possible. In a case where non-linear material response is considered, the results become more sensitive to the mesh profile and as such, it is advisable to use finer mesh profiles. The contour integral grows outwards from the crack tip to a finite region within the pipe depending on the number of output requests, and as such, it is important to read off the results from a contour that falls within the K-dominance zone. At the crack tip, the elements represented by degenerated quads should be utilised for sharp cracks. The degeneration is controlled by collapsing one side of the second-order quad elements to a single point at the crack tip and then adjusting the mid-side nodes to move closer to the crack tip by a parameter t ; arriving at a mesh that allows for accurate prediction of the stress singularity at the crack tip. Since the mid-side node parameter actively adjust the nodes on the seam elements, care should be taken when choosing its value. To avoid producing screwed elements (especially for FE 3D fracture mechanics analyses), a sensitivity study should be carried out to ascertain the minimal value for t that would not lead to analysis errors. Results outside this zone usually show inconsistency and as such should be avoided (Dassault Systèmes, 2012). It is well known that there exist an angular dependence for the stress/strain field around the crack tip and as such, we require a reasonable number of elements to obtain a good angular resolution. Subtend angles in the range of $10^\circ - 20^\circ$ around the crack tip were found to accurately obtain reasonable results for LEFM.

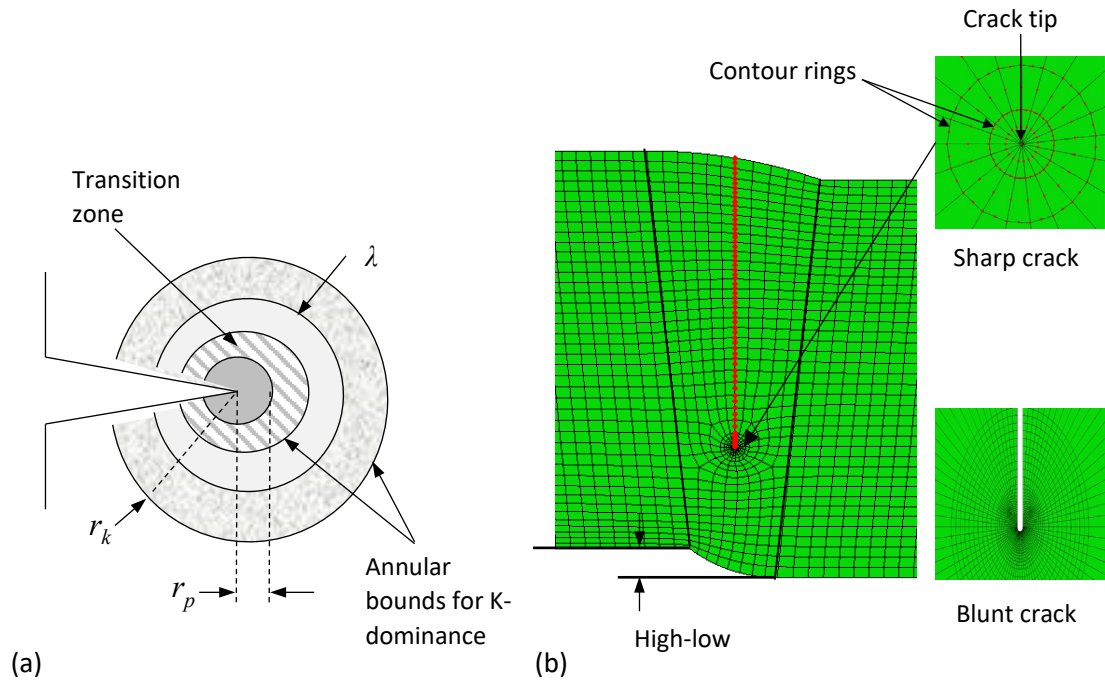


Figure 13 (a) Dominance fields (b) Validation model

5.2. Model Validation

To validate the proposed finite element methodology, a pipeline girth welded joint was modelled to replicate the analytical SIF and crack driving force solutions as outlined in DNV-GL F108 and BS 7910. Different crack depths were studied whilst also taking into consideration the influence of a 1 mm high-low characterising radial misalignment at the weld. The crack was positioned at the middle of the weld, extending through thickness as shown in Figure 13(b). The crack driving force was calculated using the expression:

$$\text{crack driving force} = \frac{K_I^2(1 - \nu^2)}{E} \cdot f(L_r) \quad (5.3)$$

Where K_I represents the mode I stress intensity factor for the flaw size and geometry considered and $f(L_r)$ is defined as in Eqn. (2.3) making it dependent on the material stress-strain curve (Figure 14b). Figure 14(a) shows the comparison between the FEA and analytical results for a full circumferential

crack in a pipe. From the results, we see that the analytical method and FEA method differ mainly in the prediction of the misalignment effect. The linear relationship between the crack driving force and the crack depth signifies that the reference stress solution remained within the elastic limit of the material for the analytical method. In addition, the analytical method does not capture the varying effect of the misalignment on the reference stress whereas the FEA method does. This explains the disparities in the results, as the FEA method captures the increased influence of the misalignment on the reference stress as the crack depth increases.

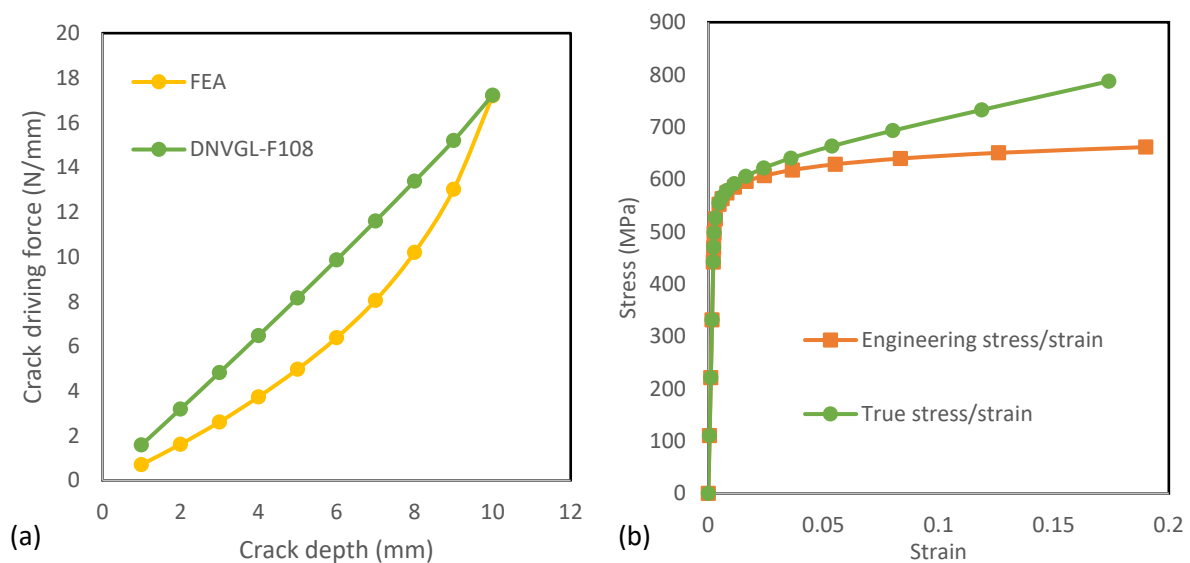


Figure 14 (a) Comparison of crack driving force results (b) Stress-strain curve

As this study focuses on installation loads, each load variant will be analysed (for SIF solutions) separately as monotonic load. The load case description are as follows:

- Full Pipe Tension (FPT): Both pipes bear the tension due to their respective submerged weights.
- Full Pipe Moment (FPM): Curvature control for sagbend.
- Installation Case (IC): External pressure, tension due to pipe weight and moment due to installation curvature; all applied as individual monotonic loads.

5.3. Swage Weld Model

The mesh profile for typical fully embedded circumferential seam crack located at the swage weld toe is presented in Figure 15. To obtain accurate contour integral results for a crack in three-dimensional analysis, care has to be taken to ensure that the mesh conforms to the cracked geometry, the crack front is explicitly defined and the appropriate virtual crack extension direction is chosen (ABAQUS, 2014). The crack front is defined as a node set and the virtual crack extension direction is specified to be orthogonal to the crack front tangent and the normal to the crack plane. Due to symmetry, only a quarter of the joint assembly was modelled. Wedge elements are created along the crack tip and a partitioning strategy ensured that the contour integral could be properly mapped within the limits for LEFM. The crack growth direction was specified to be normal to the theta plane, to ensure that the displacement vectors were captured within the rotational symmetry. C3D20 elements were used to model the joint assembly with crack line element mid-side nodes moved one-fourth points along the edge plane. Using these elements automatically implies that no mid-side nodes exist at the mid-plane and as such, no singularity would be represented within the element, which creates differences in interpolation between the mid-plane and edge planes leading to local oscillation of J-integral values along the crack line.

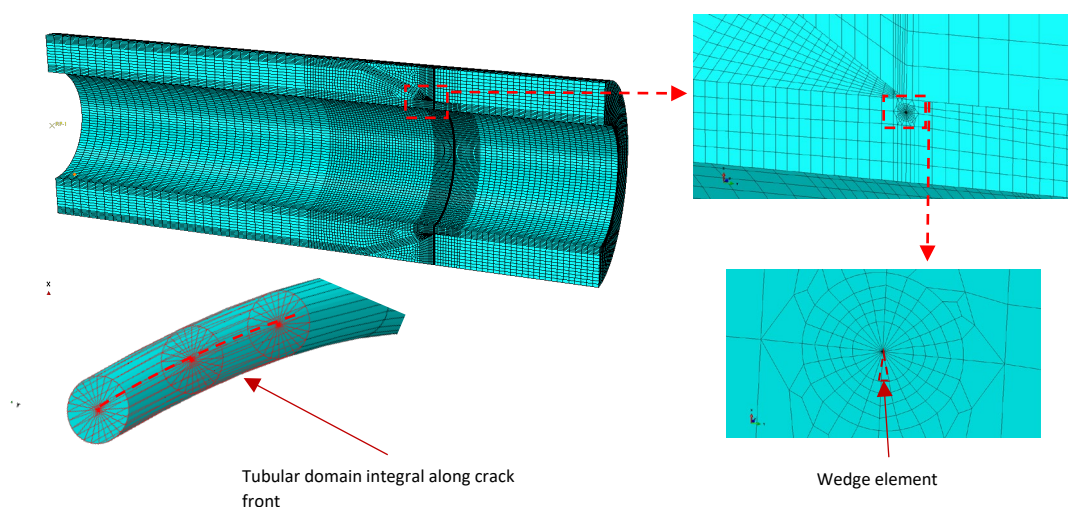


Figure 15 Swage joint mesh profile

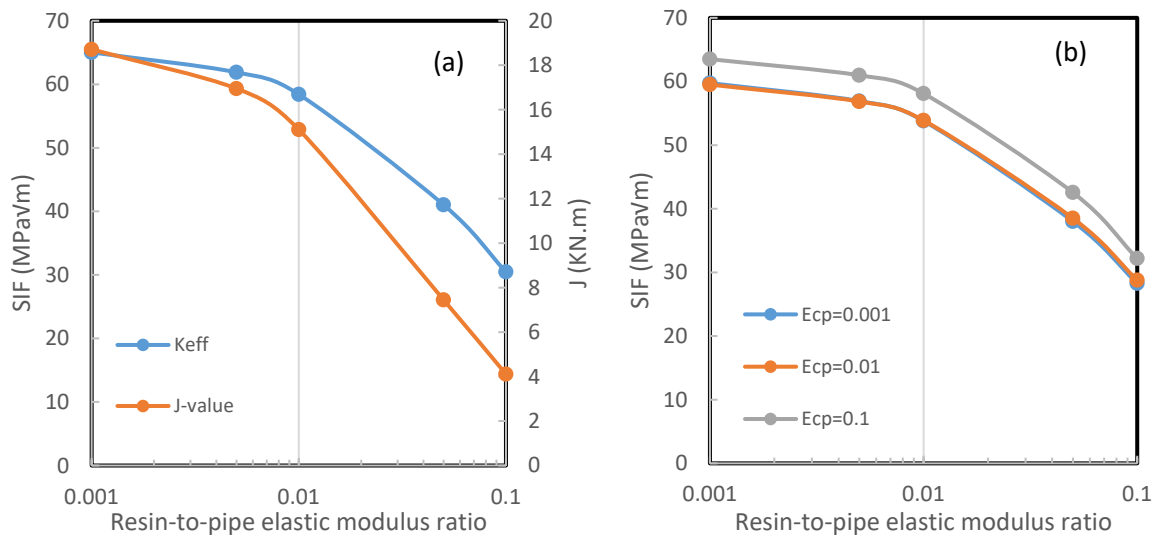
Base case installation loading on a sandwich pipe for a typical J-lay and other fixed design parameters are listed in Table 4. As mentioned earlier the loads are treated as monotonic loads applied to the joint assembly. Figure 16 shows the influence of the core-to-pipe and resin-to-pipe stiffness ratios (E_{cp} and E_{rp}) on the SIF and corresponding J-value for a sharp crack positioned at the swage weld toe of a joint assembly located at the apex of the sagbend. The J-integral and SIFs are computed directly in ABAQUS about five contour intervals and the reported values are the average of the last three intervals as the first two intervals produced significantly undulating values and as such not path independent. The contour for the extraction of the J-value (λ in Figure 13a) was chosen to fall entirely within the annular region for K-dominance.

For the modelling of isotropic materials with the perfect adhesion assumption, the load bearing capacity of the sandwich pipe joint under elastic bending load is simply the combination of the load bearing capacities of the layers. Therefore, at constant load, the influence of the core and filler resin stiffness on the elastic SIF for a crack located at the swaged weld toe can be simply quantified by the variation in stress state in the K-field domain around the crack tip. The better the load bearing properties of the annular materials, the lesser the stress state at constant load, and the lesser the elastic SIF.

The close to logarithmic relationship is expected as perfect adhesion was assumed between contacting surfaces meaning that for this ideal case of LEFM, the relative displacement of the crack faces leading to mode I, II and III opening is arrested by the consolidated interlayer stresses which are a direct function of the resin stiffness. It was also discovered, that for mode I and mode II, the elastic SIF is highest for a relatively stiffer core due to the bending stiffness mismatch effect (Onyegiri and Kashtalyan, 2017) which is more significant for discontinuous annulus type joints.

Table 4 Base case installation parameters

Parameter	Value	Unit	Comments
W_d	3000	m	Water depth
W_s	156.32	kg/m	Total submerged weight
T	5479	kN	Required top tension (Bai and Bai, 2005)
$k_{sagbend}$	0.003491	1/m	Sagbend curvature (Bai and Bai, 2005)
t_1, t_2	12.7	mm	Required wall thickness for collapse check for $E_{rp} = E_{cp} = 0.01$ (Arjomandi and Taheri, 2011)
(r_1, r_2)	(109.55,161.95)	mm	Inner and outer pipe radius
σ_y	552	MPa	Pipe yield stress
K_{mat}	65	MPa(m) ^{1/2}	Critical SIF



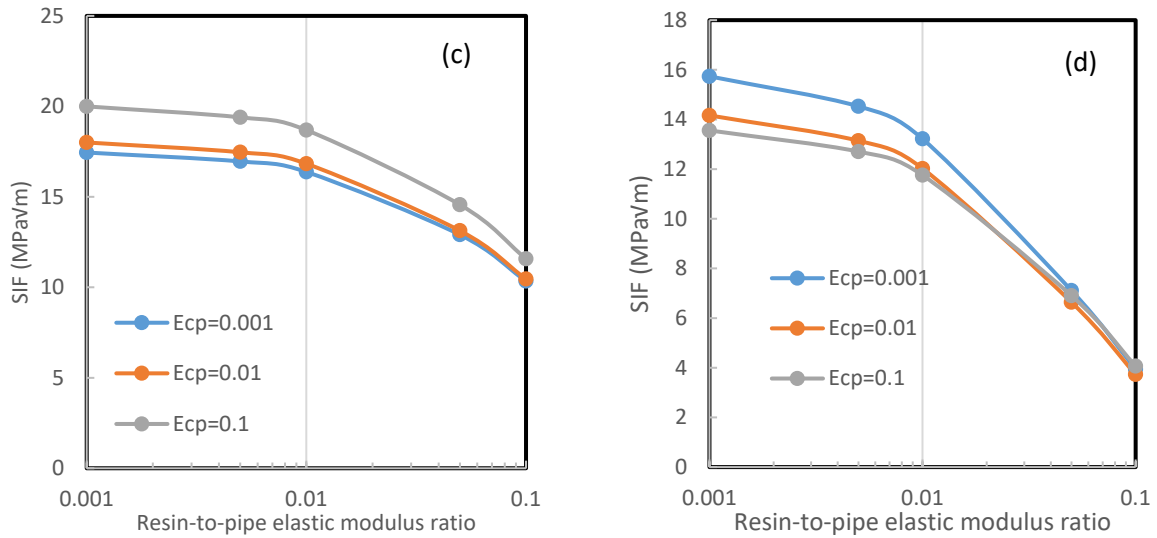


Figure 16 Influence of resin-to-pipe elastic modulus ratio E_{rp} for a range of core-to-pipe elastic modulus ratios E_{cp} on:

(a) the K_{eff} and J-integral (b) K_I (c) K_{II} (d) K_{III}

For the fully circumferential crack, the angular dependence of the J-integral can be seen in Figure 17 for a full pipe moment and full pipe tension case. For the moment case, Figure 17a, we can clearly see the symmetry about the 90° point corresponding with the typical bending stress distribution in a pipe about its neutral axis. This goes further to show that the J-value for elastic analysis is directly proportional to the crack front stress-state within the J-integral contour domain. For the tension case, Figure 17b, it is observed that the J-value remains constant as the joint assembly is subject to the uniform weight of the submerged pipe. These results prove J-integral consistency for an isotropic homogenous material evaluated using LEFM as the J-value is directly proportional to the square of the load effect, see Eqn. (5.2).

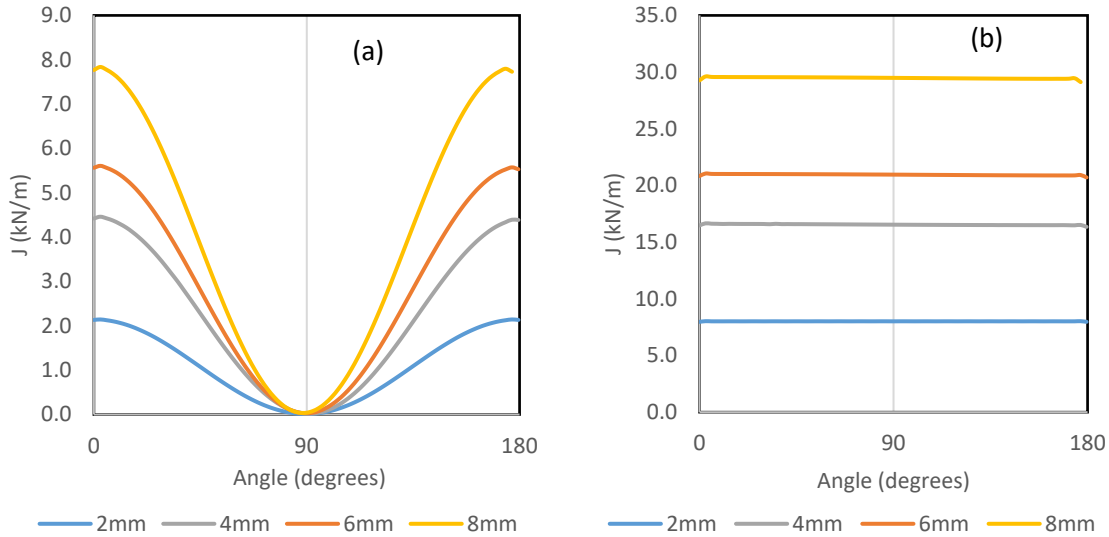


Figure 17 Angular dependence of the J-integral at different crack depths: (a) Applied moment (b) Applied tension

6. Acceptable defect criteria

To the best of the authors' knowledge, there exists no documented reference stress and stress intensity solutions for the swage weld configuration and as such, two different approaches are utilised to illustrate how an ECA can be carried out for the swage weld. The first approach is as documented in both (DNVGL-RP-F108, 2017) and (BS 7910, 2013) using the Fracture Assessment Diagram (FAD). This approach utilises a failure assessment curve to ascertain if crack growth will become unstable under a given loading condition. This approach may be used for both stress-based conditions (especially in the elastic regime) and strain-based conditions well into the plastic regime. The second approach involves using the J-integral to determine both the geometric factor and reference stress solutions of a specific crack configuration as a function of the nominal load applied; this is stipulated in Section 9G.4 of (API-579-1/ASME-FFS-1, 2016) and can be used for elastic-plastic analysis. Both approaches require the use of FEA for the swage weld joint type.

6.1. FAD approach for LEFM

The FAD approach was applied for the previously mentioned load cases (Section 5.2) for elastic analysis. The SIF solutions derived from the FEA are inputted in Eqn. (2.2) to compute the effective SIF, K_{eff} . The load ratio L_r is derived from the ratio of the reference stress σ_{ref} to the pipe yield stress σ_y . For the reference stress solution, a global pipeline model is utilised with the appropriate loading condition. The reference stress is computed as the maximum longitudinal stress averaged across K-dominance field (where the elastic SIF solutions are computed).

Figure 18 shows the influence of the loading condition on the acceptability of a defect using the FAD approach for a sandwich pipe swage joint. The assessment points are displayed for a circumferential crack with crack-to-thickness ratio, $a/t_1 = 0.3$ and the influence of the filler resin stiffness is shown. We see that the stiffness of the filler resin can alter the acceptability of an assessment point under the perfect adhesion assumption for this approach applied based on LEFM. The crack and loading conditions analogous to the points that lie within the failure assessment curve are deemed acceptable, as they would not lead to unstable crack growth. As can be inferred, this approach is better suited for brittle materials as it does not take into consideration the elastic-plastic behaviour of the pipe material.

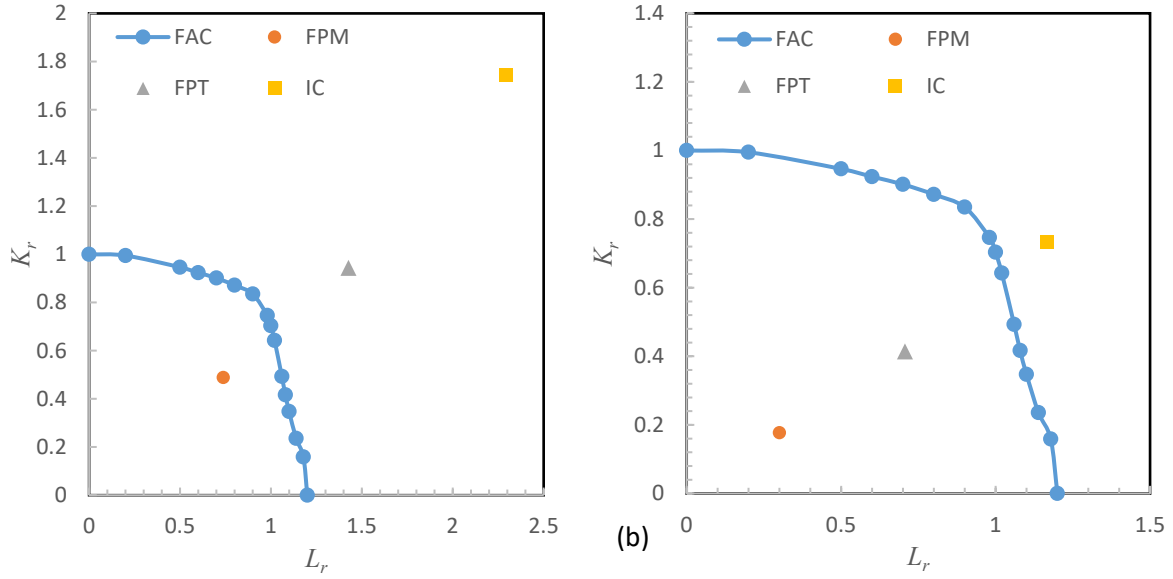


Figure 18 FAD assessment points for $a/t_1 = 0.3$: (a) $E_{rp} = 0.01$; (b) $E_{rp} = 0.1$

6.2. Geometric factor approach

The second approach involves a methodology using the J-integral results from elastic-plastic analysis to determine the geometric factor and reference stress. A full description of the generic approach can be found in Section 9G.4 of (API-579-1/ASME-FFS-1, 2016). Using the finite element method, the J-total values are computed as a function of the applied load as seen in Figure 19a for the base case model with $a/t_1 = 0.3$, from which the equivalent total SIF, K_{eqv} is computed from Eqn. (2.6) by replacing K_{mat} with K_{eqv} and J_{mat} with J-total. To determine the fracture ratio, K_r , we compute the equivalent elastic J-integral and thus the elastic K solution by curve fitting the near-linear portion of the J-total plot. We know this to be true because for elastic behaviour the J-integral is proportional to the square of the load, thus allowing us to use a simple power law correlation to express the first four points of J-total.

$$J\text{-elastic}_i = 1.028 * \text{applied load}_i^{2.002} \quad i = \text{data points} \in J\text{-total} \quad (6.1)$$

An elastic K is then calculated from Eqn. (2.6) by replacing J_{mat} with J-elastic. To further verify this, if the proper stress-strain curve has been utilised for the FEA, the fitted J-elastic will start to show significant divergence from J-total around the critical J-value for the material, J_{mat} . This also means

that, as plasticity increases at the crack front, the divergence increases, inferring that J-total is a function of the load and crack dimension. The method specific fracture ratio K_r^* , is then expressed as the ratio between the elastic K and K_{eqv} and plotted against the applied load as seen in Figure 19b. We then derive the material specific K_r value (similar to K_r at $L_r = 1$ from material specific FAC in (BS 7910, 2013) from the (API-579-1/ASME-FFS-1, 2016) equation 9G.3:

$$K_r^{L_r=1} = \left(\sqrt{1 + \frac{0.002E}{\sigma_y}} + 0.5 \left(1 + \frac{0.002E}{\sigma_y} \right)^{-1} \right)^{-1} \quad (6.2)$$

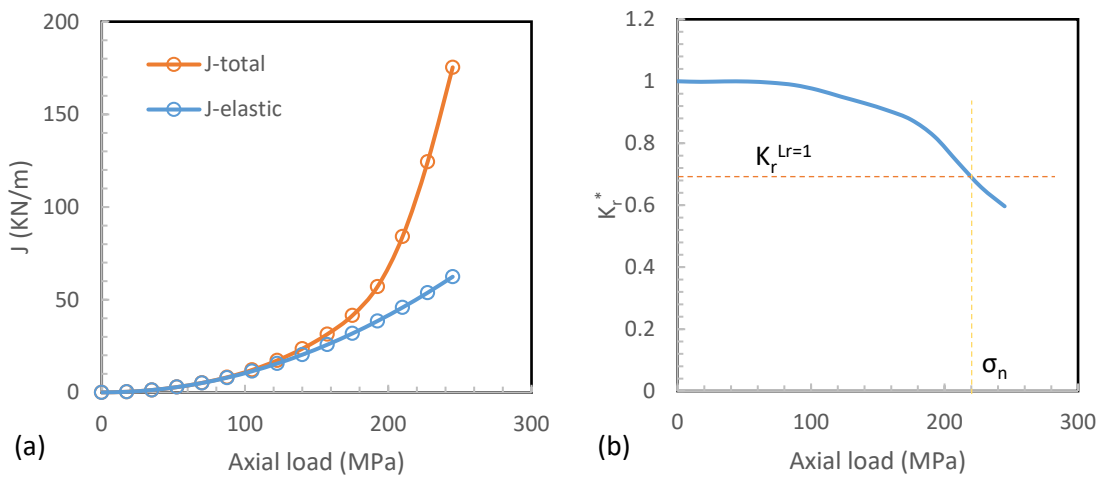


Figure 19 (a) J-total, J-elastic for $a/t_1 = 0.3$ under axial loading (b) Nominal load at material specific K_r

The intersection of $K_r^{L_r=1}$ with K_r^* gives us the nominal load σ_n unique to this joint configuration and crack dimension from which we derive the geometric factor F_{ref} using:

$$F_{ref} = \frac{\sigma_y}{\sigma_n} \quad (6.3)$$

Furthermore, we see that the geometric factor is a function of the crack dimensions and allows us to calculate the reference stress for any specific load σ_d applied to the sandwich pipe joint using:

$$\sigma_{ref} = F_{ref} \sigma_d \quad (6.4)$$

The advantage of this approach is its capability to be used for a variety of structural geometries and crack locations, even more so in scenarios where existing reference stress and stress intensity solutions are not available (Thorwald and Vargas, 2017). Figure 20a shows the influence of the crack to pipe thickness ratio (a/t_1) on F_{ref} for a circumferential swage weld toe crack in a sandwich joint assembly. In contrast, for the loading cases, we can see that F_{ref} shows stronger dependence on a/t_1 for isolated monotonic loads. The simulated installation case (a combination of monotonic load steps) shows lesser dependence mainly due to the hydrostatic loading. This is because it is assumed that the friction between the pipe and seabed is large enough to restrict lateral and longitudinal movement at the touchdown point, which means the hydrostatic pressure acting on the joint assembly will induce compressive stresses on the inner pipe. These stresses are further relieved by the axial stress induced due to the pipe's weight and bending stress at tensile side of the sagbend. It should be mentioned here that the isolated load cases give a geometric factor at an equivalent stress value where we can extract the nominal load for the lowest studied a/t_1 value. For example, for the curvature control load step (FPM case), we can see that an equivalent bending stress value of 322MPa needs to be attained whereas an equivalent axial stress of 245MPa needs to be attained for the tension load case. The influence of material plasticity on the acceptability of an assessment point is shown in Figure 20b as contrasted with the failure assessment curve (BS 7910, 2013) from the elastic analysis. Four different assessment points are considered at constant bending moment applied to the joint assembly. It can be seen that if we consider plasticity in the development of the failure assessment curve, the $a/t_1 = 0.63$ assessment point would be deemed acceptable. In the absence of any code or standard, that provides procedural guidance for the fracture toughness testing and fatigue crack growth rate testing of the sandwich pipe swage joint geometry, the ECA via FE elastic-plastic analysis provides the general assessment procedure.

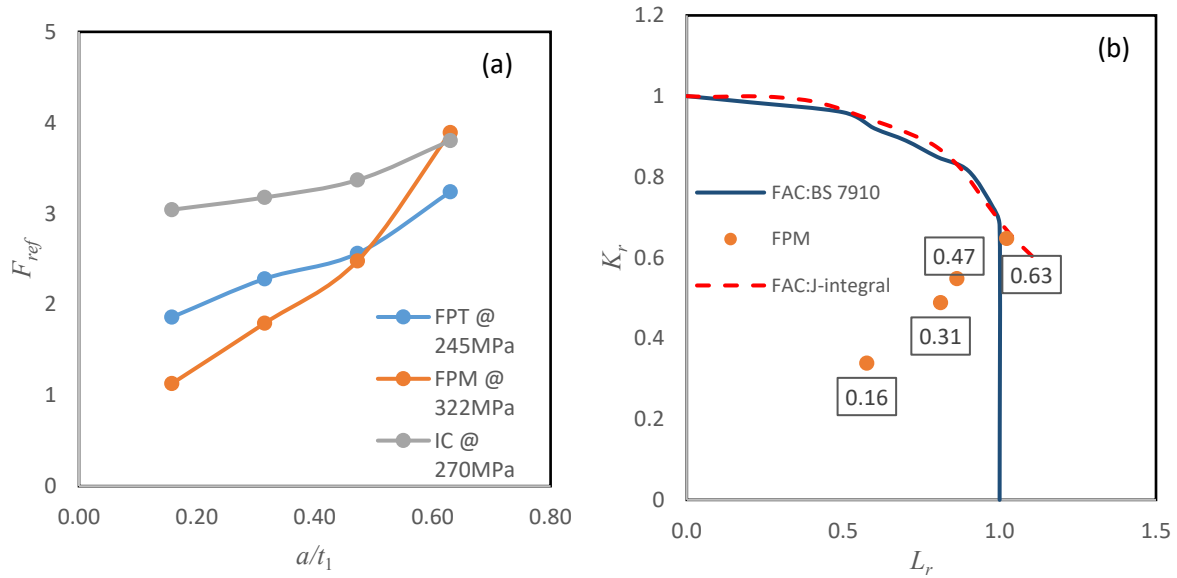


Figure 20 (a) Influence of the crack depth/inner pipe thickness ratio on the geometric factor; (b) Influence of plasticity on the acceptability criteria for assessment points

7. Conclusions

Sandwich pipes have been shown to be a viable solution to both the thermal insulation and weight requirement constraints for deepwater installation. To ensure these benefits, the integrity of the sandwich pipe swage welds need to be preserved and this calls for, in most cases, bespoke solutions due to the geometry and loading type. This also means that a certified non-destructive examination procedure needs to be developed that adequately covers practical areas for sandwich pipe utilisation.

This paper has focused on the engineering critical assessment of the swaged weld of a sandwich pipe joint. It follows a fitness-for-purpose acceptance criteria based on FE fracture mechanics analysis, with the main conclusions being:

- For a defect free model, the swaged weld was shown to be a stress raiser and the stress distribution around the swage weld was visualized using finite element models. For the range of elastic modulus ratios studied, results showed the weld toe to be the location of the greatest stress discontinuity and thus the critical defect location under installation type loading.

- For elastic analysis, parametric studies showed that the swaged weld dimensions are critical design variables that influence the stress distribution around the joint. The stress concentration factor at the swaged weld toe has a direct proportional relationship to the weld gap w_g and weld-to-pipe elastic modulus ratio E_{wp} and an inverse relationship to the weld length w_l and thickness-to-radius ratio t_1/r_1 .
- A set of parametric correlations are derived from results of 12500 FE models to express the relationship between the swage weld dimensions, elastic material properties and SCF for an axial loading case with perfect adhesion between all layers. Another set of parametric correlations were derived for the through thickness stress profile at the weld toe. Random design sets of model parameters were used to check the accuracy of the fitted equations to the FE models, with the largest error being 13.9% within the validity of the correlations.
- The FE fracture mechanics analysis is ideal for determining the acceptable defect size for the swage weld. Reference stress solutions can be extracted by the direct stress linearization of FEA results at the location of interest. The FE fracture mechanics analysis has the added advantage over analytical solutions, in that it captures the direct influence of a stress raiser (e.g high-low) on the stress distribution around the defect. It also captures how this influence varies due to the proximity of the stress raiser and the defect dimensions.
- For the modelling of isotropic materials with the perfect adhesion assumption, the better the load bearing properties of the annular materials, the lesser the stress state at constant load, and the lesser the elastic stress intensity factor for a swaged weld toe defect. J-value computation for elastic analysis is a directly proportional to the crack front stress-state within the contour domain.
- For design against plastic collapse, the FE fracture mechanics assessment outlined in (DNVGL-RP-F108, 2017) can be adopted for the swaged weld; with the aid of FEA to accurately predict the reference stress due to maximum potential loading during installation and a FAD to assess the maximum acceptable defect sizes. The methodology is also

applicable for elastic-plastic analysis, where it was shown that designing with plasticity considerations (e.g. strain-based design) indeed has an influence on the acceptability of a defect size. This sheds light to the conservative nature of brittle fracture design for materials with significant ductility.

- For elastic-plastic fracture assessment, the FE fitness-for-service approach for components with cracks outlined in (API-579-1/ASME-FFS-1, 2016) yields geometric factors for the swaged weld geometry and load case which can be used to compute the reference stress solution. The geometric factor for the swaged weld toe increases as a/t_1 increases for all potential load cases during installation.

A conservative form of assessment has been applied for the two approaches mainly because of the weighty analysis involved in arriving at correlations for the unique swage joint. Further works are encouraged especially in quantifying the influence of the core and filler properties on the fracture mechanics inputs needed to carry out an engineering critical assessment for the joint. In addition, the influence of the interlayer properties between the pipe/core and pipe/resin is unknown as all studies were carried out assuming perfect adhesion. Although we know from theory that high welding residual stress can exist in joints, and in-play, modify the reference stress and stress profile at the crack tip, the effect of welding residual stress was not captured in this study. In addition, the study only considers monotonic loads for an installation case and further works into fatigue loading are highly recommended.

Acknowledgements

The authors would like to acknowledge the financial support of the University of Aberdeen, through the Elphinstone PhD Studentship, and the support of the Maxwell computer cluster funded by the University of Aberdeen.

References

- ABAQUS 2014. ABAQUS User's and Theory Manuals. Version 6.14 ed.: Dassault.Systèmes.
- API-579-1/ASME-FFS-1 2016. Fitness-For-Service. *Annex 9G, Section 9G-4, Finite Element Analysis of Components with Cracks*. Washington D.C 20005: API Publishing Services.
- API-RP-1111 2015. Design, Construction, Operation and Maintenance of Offshore Hydrocarbon Pipelines (Limit State Design) 5th Edition. American Petroleum Institute: API Publishing Services.
- ARJOMANDI, K. & TAHERI, F. 2011. A new look at the external pressure capacity of sandwich pipes. *Marine Structures*, 24, 23-42.
- ARUN, S., SHERRY, A. H., SMITH, M. C. & SHEIKH, M. 2014. Finite Element Simulation of a Circumferential Through-Thickness Crack in a Cylinder. V003T03A086-C1 - Volume 3: Design and Analysis.
- ASME BPVC-VIII-2 2015. Rules for Construction of Pressure Vessels Division 2-Alternative Rules. NY, USA: American Society of Mechanical Engineers, ASME.
- BAI, Y. & Q., B. 2005. Limit-state based Strength Design. In: Y., B. & Q., B. (eds.) *Subsea Pipelines and Risers*. Oxford: Elsevier Science Ltd.
- BAI, Y. & BAI, Q. 2005. Installation Design. In: Y, B. & Q, B. (eds.) *Subsea Pipelines and Risers*. Oxford: Elsevier Science Ltd.
- BELL, R., CANADA CENTRE FOR MINERAL AND ENERGY, T. & CARLETON UNIVERSITY. FACULTY OF, E. 1985. *Determination of Stress Intensity Factor for Weld Toe Defects, Phase II: Final Report*, Carleton University, Faculty of Engineering.
- BJERKE, S. L., SCULTORI, M. & WÄSTBERG, S. 2011. DNV's Strain-based Fracture Assessment Approach for Pipeline Girth Welds. *International Offshore and Polar Engineering Conference*. Maui, Hawaii, USA: ISOPE.
- BS 7910 2013. Guide to Methods for Assessing the Acceptability of Flaws in Metallic Structures. *Assessment for Fatigue; Assessment for Fracture Resistance* British Standards Publication.
- DASSAULT SYSTÈMES 2012. *Modeling Cracks & Fracture Analysis*, MA, USA, Dassault Systèmes Americas Corp.
- DIXON, M., JACKSON, D. & EL CHAYEB, A. 2003. Deepwater Installation Techniques for Pipe-in-Pipe Systems Incorporating Plastic Strains. *Offshore Technology Conference*. Houston, Texas: Offshore Technology Conference.
- DNV-OS-F101 2007. Submarine pipeline systems. *Appendix A: Structural Integrity of Pipeline Girth Welds in Offshore Pipelines* Det Norske Veritas AS.
- DNV-RP-A203 2011. Qualification of New Technology. Norway: DNV, Det Norske Veritas AS.
- DNVGL-RP-F108 2017. Assessment of flaws in pipeline and riser girth welds. *Use of Finite Element Fracture Mechanics Analyses to Assess Maximum Allowable Flaw Sizes*. DNV GL AS.
- IRWIN, G. R. 1961. Plastic zone near a crack and fracture toughness. In: Mechanical and metallurgical behavior of sheet materials. *7th Sagamore Ordnance Materials Research*, 63-78.
- JONES, R. L., GEERTSEN, C., BOOTH, P., MAIR, J. A., SRISKANDARAJAH, T. & RAO, V. 2013. Pipe-in-Pipe Swaged Field Joint for Reel Lay. *Offshore Technology Conference*. Houston, Texas, USA: OTC.

- KIBEY, S., WANG, X., MINNAAR, K., MACIA, M. L., FAIRCHILD, D. P., KAN, W. C., FORD, S. J. & NEWBURY, B. 2010. Tensile Strain Capacity Equations for Strain-Based Design of Welded Pipelines. 355-363
- C1 - 2010 8th International Pipeline Conference, Volume 4.
- KYRIAKIDES, S. & CORONA, E. 2007. 2 - Offshore Facilities and Pipeline Installation Methods. *In: CORONA, S. K. (ed.) Mechanics of Offshore Pipelines*. Oxford: Elsevier Science Ltd.
- MALLIK, A., ATIN, C., WANG, J., DELEYE, X. & LEGRAS, J.-L. 2013. Control of the Integrity of Swaged Weld on Insulated Pipe-in-Pipe. *Offshore Technology Conference*. Houston, Texas, USA: OTC.
- MORGAN, M. R. & LEE, M. M. K. 1998. Parametric equations for distributions of stress concentration factors in tubular K-joints under out-of-plane moment loading. *International Journal of Fatigue*, 20, 449-461.
- ONYEGIRI, I. & KASHTALYAN, M. 2017. Finite element analysis of a sandwich pipe joint. *Ocean Engineering*, 146, 363-374.
- OSTBY, E. 2005. Fracture Control — Offshore Pipelines: New Strain-Based Fracture Mechanics Equations Including the Effects of Biaxial Loading, Mismatch, and Misalignment. 649-658. C1 - 24th International Conference on Offshore Mechanics and Arctic Engineering: Volume 3.
- PISARSKI, H. 2011. Assessment of Flaws in Pipe Girth Welds. *CBMM-TMS International Conference on Welding of High Strength Pipeline Steels*. Araxá, Brasil.
- PISARSKI, H., XU, G. & SMITH, S. 2006. Fracture mechanics assessment of flaws in pipeline girth welds. *International Seminar on Application of High Strength Line Pipe And Integrity Assessment of Pipeline*. Xi'an, China: HSLP-IAP.
- SIGMAPLOT 2014. Version 13 ed. San Jose, CA, USA: Systat Software Inc.
- SUN, C. T. & JIN, Z. H. 2012. Chapter 3 - The Elastic Stress Field around a Crack Tip. *In: SUN, C. T. & JIN, Z. H. (eds.) Fracture Mechanics*. Boston: Academic Press.
- THORWALD, G. & VARGAS, P. 2017. Cylinder Axial Crack Reference Stress Comparison Using Elastic-Plastic FEA 3D Crack Mesh J-Integral Values. V03BT03A031-C1 - Volume 3B: Design and Analysis.
- VITALI, L., BRUSCHI, R., MORK, K. J., LEVOLD, E. & VERLEY, R. 1999. Hotpipe Project: Capacity of Pipes Subject to Internal Pressure, Axial Force And Bending Moment. International Society of Offshore and Polar Engineers.
- YOO, A. B., JETTE, M. A. & GRONDONA, M. SLURM: Simple Linux Utility for Resource Management. *In: FEITELSON, D., RUDOLPH, L. & SCHWIEGELSHOHN, U., eds. Job Scheduling Strategies for Parallel Processing, 2003// 2003 Berlin, Heidelberg*. Springer Berlin Heidelberg, 44-60.
- ZEHNDER, A. T. 2012. *Fracture Mechanics*, Dordrecht, Netherlands, Springer.
- ZHU, X.-K. & JOYCE, J. A. 2012. Review of fracture toughness (G, K, J, CTOD, CTOA) testing and standardization. *Engineering Fracture Mechanics*, 85, 1-46.